AGU PUBLICATIONS

JGR

Journal of Geophysical Research: Space Physics

RESEARCH ARTICLE
10.1002/2014JA020729

Key Points:
- There are three widely used internal Jovian magnetic field models
- We compare auroral mapping results using different field models
- Mapping results can be shifted by several degrees or tens of Jovian radii

Correspondence to:
M. F. Vogt,
mvogt@bu.edu

Citation:
Vogt, M. F., E. J. Bunce, M. G. Kivelson, K. K. Khurana, R. J. Walker, A. Radioti, B. Bonfond, and D. Grodent (2015), Magnetosphere-ionosphere mapping at Jupiter: Quantifying the effects of using different internal field models, *J. Geophys. Res. Space Physics*, *120*, 2584–2599, doi:10.1002/2014JA020729.

Received 13 OCT 2014
Accepted 24 FEB 2015
Accepted article online 28 FEB 2015
Published online 13 APR 2015

Magnetosphere-ionosphere mapping at Jupiter: Quantifying the effects of using different internal field models

Marissa F. Vogt[1,2], Emma J. Bunce[3], Margaret G. Kivelson[4,5], Krishan K. Khurana[4], Raymond J. Walker[4,6], Aikaterini Radioti[7], Bertrand Bonfond[7], and Denis Grodent[7]

[1]Center for Space Physics, Boston University, Boston, Massachusetts, USA, [2]Previously at Department of Physics and Astronomy, University of Leicester, Leicester, UK, [3]Department of Physics and Astronomy, University of Leicester, Leicester, UK, [4]Department of Earth, Planetary, and Space Sciences, UCLA, Los Angeles, California, USA, [5]Department of Atmospheric, Oceanic, and Space Science, University of Michigan, Ann Arbor, Michigan, USA, [6]Previously at National Science Foundation, Arlington, Virginia, USA, [7]LPAP, Université de Liège, Liege, Belgium

Abstract The lack of global field models accurate beyond the inner magnetosphere ($<30\ R_J$) makes it difficult to relate Jupiter's polar auroral features to magnetospheric source regions. We recently developed a model that maps Jupiter's equatorial magnetosphere to the ionosphere using a flux equivalence calculation that requires equal flux at the equatorial and ionospheric ends of flux tubes. This approach is more accurate than tracing field lines in a global field model but only if it is based on an accurate model of Jupiter's internal field. At present there are three widely used internal field models—Voyager Io Pioneer 4 (VIP4), the Grodent Anomaly Model (GAM), and VIP Anomaly Longitude (VIPAL). The purpose of this study is to quantify how the choice of an internal field model affects the mapping of various auroral features using the flux equivalence calculation. We find that different internal field models can shift the ionospheric mapping of points in the equatorial plane by several degrees and shift the magnetospheric mapping to the equator by ~30 R_J radially and by less than 1 h in local time. These shifts are consistent with differences in how well each model maps the Ganymede footprint, underscoring the need for more accurate Jovian internal field models. We discuss differences in the mapping of specific auroral features and the size and location of the open/closed field line boundary. Understanding these differences is important for the continued analysis of Hubble Space Telescope images and in planning for Juno's arrival at Jupiter in 2016.

1. Introduction

Jupiter's ultraviolet auroral emissions were first observed during the Voyager 1 flyby [*Broadfoot et al.*, 1979]. In the decades since, ground- and space-based telescopes, most notably the Hubble Space Telescope (HST), have produced dazzling, high-resolution images of Jupiter's aurora. These observations provide an excellent tool for global studies of Jupiter's magnetosphere because the auroral zone responds to activity occurring simultaneously across a large range of radial distances and local times in near equatorial regions, whereas in situ measurements are generally available only at a single location in the magnetosphere [e.g., *Gérard et al.*, 2013]. Determining the physical processes that produce features in Jupiter's aurora requires a reliable way to link a specific position in the ionosphere to a source region in the magnetosphere. Unfortunately, the accuracy of the available global field models is insufficient to reliably map between the polar ionosphere and the middle to outer magnetosphere by tracing model field lines. Therefore, *Vogt et al.* [2011] developed a mapping model that uses a flux equivalence calculation, which relates the magnetic flux measured at a given radial distance and local time in the equatorial magnetosphere to the equivalent magnetic flux in the ionosphere.

While *Vogt et al.*'s [2011] flux equivalence mapping is more accurate, particularly in the outer magnetosphere, than tracing field lines from a global field model, the calculation still requires the use of a Jovian internal magnetic field model, and such models introduce uncertainty. There are three widely utilized Jovian internal field models: Voyager Io Pioneer 4 (VIP4) [*Connerney et al.*, 1998], the Grodent Anomaly Model, which we refer to as GAM [*Grodent et al.*, 2008b], and VIP Anomaly Longitude (VIPAL) [*Hess et al.*, 2011]. All three models employ the auroral footprints of one or more of the Galilean moons to constrain the properties of the internal

field at low latitudes. The models differ, sometimes significantly, in the predicted mapping of the Ganymede footprint and the strength of the radial component of the internal field, two features that are central to the flux equivalence calculation.

The purpose of this study is to investigate how the choice of an internal field model affects the flux equivalence calculation and the mapping of various auroral features. We quantify the difference in the mapping of specific locations and in the size and location of the predicted open/closed field line boundary. It is important to understand how the choice of internal field model affects the mapping results, because the differences reveal the scale of uncertainties in the mapping. For example, depending on the internal field model adopted, auroral flares or spots may map to different magnetospheric positions with respect to boundaries like the magnetopause or a statistical X line, results that could change the interpretation of the underlying physical processes. Mapping uncertainties should be taken into account in the continued analysis of HST images and in planning observations for the Juno mission scheduled to arrive at Jupiter in 2016 [*Bagenal et al*., 2014].

We begin with a review of *Vogt et al*.'s [2011] flux equivalence mapping method and its assumptions in section 2. We discuss the VIP4, GAM, and VIPAL internal field models in section 3. In section 4 we present an overview of the auroral mapping results calculated using the different field models and compare mappings of specific auroral features. We conclude with a summary.

2. Mapping by Flux Equivalence: Methods, Applications, and Limitations

The flux equivalence mapping model developed by *Vogt et al*. [2011] links polar auroral features to the equatorial magnetosphere using an approach that is more accurate than tracing field lines in available global field models, which are unreliable beyond ~30 R_J (1 Jovian radii, 1 $R_J = 71492$ km). Existing global field models include the contributions from Jupiter's internal magnetic field and the field perturbations associated with the magnetospheric current sheet and magnetopause currents. The internal field models rely on the Galilean satellites' ionospheric footprints to verify their accuracy in the inner magnetosphere. However, no satellite footprints are available to constrain the full models in the middle and outer magnetosphere, so the accuracy of field line tracing from a global model cannot be verified. *Cowley and Bunce* [2001] employed a flux equivalence analysis to estimate currents and magnetically map Jupiter's ionosphere, but they used a simplified axisymmetric field, neglecting important dawn-dusk asymmetries that have been observed in the magnetic field in the middle and outer magnetosphere [e.g., *Khurana*, 2001; *Kivelson and Khurana*, 2002]. A key contribution of *Vogt et al*.'s [2011] model is that it accounts for these dawn-dusk asymmetries by quantifying the distribution of equatorial magnetic flux across the magnetosphere as a function of both radial distance and local time based on fits to spacecraft observations. Results of the mapping model can be accessed via a webform at http://www.igpp.ucla.edu/people/mvogt/mapping/, which has recently been updated to include the flux equivalence calculation using the VIP4 internal field model in the northern hemisphere and VIPAL in both hemispheres described here.

We briefly summarize *Vogt et al*.'s [2011] method here and refer the reader to that paper for further details. The flux equivalence calculation is based on the requirement that the magnetic flux through a given region in the ionosphere must equal the magnetic flux through the region to which it maps in the magnetosphere. Calculating the flux at the equator requires knowledge of $B_{N,\mathrm{eq}}$, the component of the magnetic field normal to the current sheet, as a function of radial distance and local time, and calculating the flux through the ionosphere requires knowledge of the ionospheric radial field, $B_{R,\mathrm{ion}}$, from a model of Jupiter's internal field. *Vogt et al*. [2011] estimated $B_{N,\mathrm{eq}}$ from a two-dimensional fit to magnetometer observations acquired at varying solar wind conditions and assumed $B_{R,\mathrm{ion}}$ from the Grodent Anomaly Model (GAM) [*Grodent et al*., 2008b] in the northern hemisphere and VIP4 [*Connerney et al*., 1998] in the southern hemisphere (see section 3).

The mapping procedure is illustrated in Figure 1. It begins by tracing model field lines to the ionosphere from 15 R_J in the equator, where field models can be checked against the Ganymede footprint. The mapping procedure continues by calculating the amount of flux through the equator, in 5 R_J increments through the magnetosphere, from the starting point at 15 R_J to 150 R_J. The mapping from 15 to 20 R_J is determined by starting with the 15 R_J ionospheric reference contour and moving normal to it, tangent to the surface, until

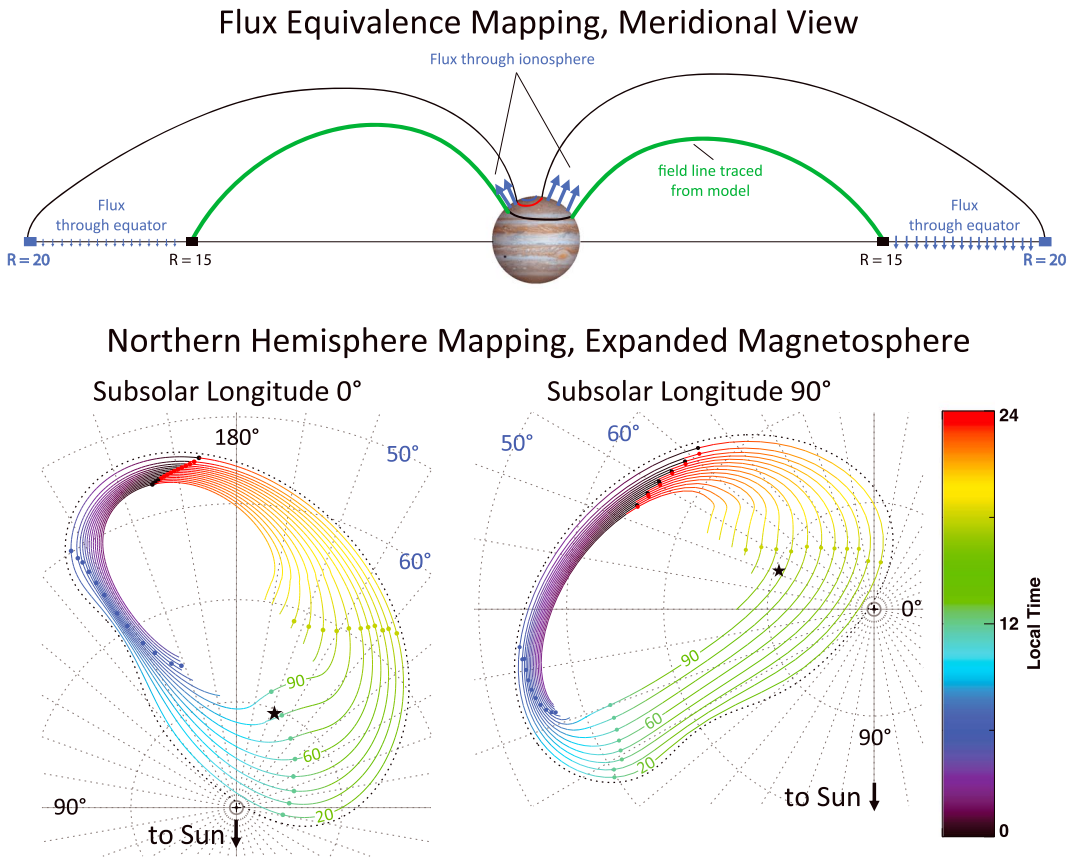

Figure 1. (top) Illustration of the flux equivalence mapping procedure shown here in the meridian plane. The initial 15 R_J ionospheric contour is determined by tracing a model field line from the equator. The positions of additional ionospheric contours mapping to larger equatorial distances are determined by moving poleward until the flux through the ionosphere matches the flux through the equator in the relevant region (i.e., from 15 to 20 R_J as shown). Modified from *Vogt et al.* [2011, Figure 4]. (bottom) Northern hemisphere ionospheric contours, each mapping to a constant radial distance in the magnetosphere, with color indicating the mapped local time. The outer black dashed line shows the initial 15 R_J reference contour. The small colored circles indicate the mapped locations of midnight, dawn, noon, and dusk local times. This mapping assumed the GAM internal field in the ionosphere. The Sun's direction is to the bottom of the page, dawn is to the left, and dusk is to the right. For reference, the system III (left handed) longitude is labeled in black, and latitude is labeled in blue. Modified from *Vogt et al.* [2011, Figure 9].

the flux through the ionosphere matches the flux through the equator from 15 to 20 R_J. Successive iterations complete the mapping out to 150 R_J. The result is a series of ionospheric contours, each of which maps to a constant radial distance in the magnetosphere. Because of the ~10° tilt of Jupiter's magnetic dipole and, in the northern hemisphere, the presence of a magnetic anomaly in the "kink" region, the mapping is highly dependent on subsolar longitude, which sets the relationship between jovigraphic longitude and local time. In the flux equivalence calculation and in the mapping results presented here, we approximate Jupiter's oblate surface (radius ~0.935–0.9585 R_J over the area of interest in the northern hemisphere) as a sphere with radius 0.95 R_J.

Figure 1 (bottom) shows a sample set of mapped ionospheric contours from the mapping model of *Vogt et al.* [2011], obtained by using the GAM internal field in the northern hemisphere. Each ionospheric contour maps to a constant radial distance in the magnetosphere. The contours are drawn in 10 R_J increments, from 20 R_J to either the dayside magnetopause (following *Joy et al.* [2002]) or to 150 R_J on the nightside, and the color indicates the mapped local time in the magnetosphere. Because $B_{N,\mathrm{eq}}$ is largest on the dusk side, the magnetic flux through a given area in the equator is also largest on the dusk side, meaning that the ionospheric contours must be farther apart where they map to dusk than where they map to dawn (assuming that $B_{R,\mathrm{ion}}$ is roughly constant).

The mapping model is useful for linking polar auroral features or regions to their source regions in the magnetosphere. For example, the polar UV auroral emissions can be classified into three regions according to their average brightness and temporal variability [*Grodent et al*., 2003b]. The active region is located poleward of the main oval near noon and is characterized by bright spots and flares. The so-called "dark region" is a crescent-shaped area that appears dark in the UV and is located immediately poleward of the main oval at dawn to prenoon local times. Finally, the swirl region is located poleward of the dark and active regions and is characterized by patchy, swirling emissions. Many interpretations of each region have been proposed [e.g., *Pallier and Prangé*, 2001; *Waite et al*., 2001; *Grodent et al*., 2003b; *Cowley et al*., 2003; *Stallard et al*., 2003; *Bunce et al*., 2004] as reviewed by *Grodent* [2014]. Using the flux equivalence mapping method, *Vogt et al*. [2011] were able to confirm the interpretation of the swirl region as Jupiter's polar cap, as much of it maps to open field lines beyond 150 R_J on the night side and that the active region maps to open field lines near and beyond the dayside magnetopause and therefore is likely a signature of the polar cusp. The mapping of the dark region is less certain, as the shape and location of the three regions shift with time. In one auroral image, the dark region appeared to map to predawn open field lines, while in another, the dark region mapped to a region which straddled both open and closed field lines near dawn local times.

The mapping model has also been used to identify the source regions of polar dawn spots, which are transient emissions that appear with a characteristic recurrence time of a few days [*Radioti et al*., 2008b]. These spots are thought to be associated with inward flow from a tail reconnection site because of their emitted power, recurrence time, and observed location [*Radioti et al*., 2010], since most in situ reconnection signatures have been reported in the predawn local time sector [*Kronberg et al*., 2005; *Vogt et al*., 2010]. Similar spots have been reported in the nightside aurora. *Radioti et al*. [2011] reported on HST observations showing a nightside auroral spot that maps, using the flux equivalence calculation, very close to the position of the Galileo spacecraft, which recorded a magnetic field dipolarization suggestive of tail reconnection at nearly the same time. The mapping of polar dawn spots is discussed further in section 4.2.

While the flux equivalence calculation represents an improvement over tracing field lines from a global model, it has evident limitations. One major source of error in the mapping model is the use of a time-averaged $B_{N,\mathrm{eq}}$, as there are important temporal variations that are not taken into account. The field strength is known to change in response to a magnetospheric compression by the solar wind [e.g., *Hanlon et al*., 2004; *Tao et al*., 2005], so using a fit to $B_{N,\mathrm{eq}}$ that is averaged over all solar wind conditions introduces an error that is particularly important when mapping auroral features from specific observations made under particular (usually unknown) solar wind conditions. Additionally, models and data suggest that variability in the plasma mass loading rate from Io can change the field configuration in the middle magnetosphere and shift the main emission and Ganymede footprint by a few degrees on time scales of months [e.g., *Russell et al*., 2001; *Grodent et al*., 2008a; *Nichols*, 2011; *Bonfond et al*., 2012]. This temporal variation would influence the flux equivalence calculation because it affects both the initial 15 R_J reference contour and $B_{N,\mathrm{eq}}$. The other major source of error in the mapping model is the internal field model used to determine $B_{R,\mathrm{ion}}$ in calculating the flux through the ionosphere and to locate the 15 R_J reference contour near the Ganymede footprint. This second error is the topic of the present study.

3. Available Internal Magnetic Field Models

As discussed above, there are three widely used models of the Jovian internal magnetic field: VIP4, GAM, and VIPAL. All employ the auroral footprints of one or more of the Galilean moons to constrain the properties of the field at relatively low latitudes. In each case, the full model field is given by the internal field plus the contribution of a current sheet [*Connerney et al*., 1981, 1998]. Emissions have been observed at the ionospheric footprints of Io (5.9 R_J), Europa (9.4 R_J), and Ganymede (15 R_J) [*Connerney et al*., 1993; *Clarke et al*., 2002] (see review by *Bonfond* [2013]). The footprints provide key constraint to internal field models because the satellites' orbital locations are known, making it possible to reliably link a footprint's ionospheric location to a radial distance in the equatorial magnetosphere. There is a small uncertainty (~1–2 h of local time) due to the signal propagation time between the satellite and Jupiter's ionosphere.

The VIP4 internal field model [*Connerney et al*., 1998] was developed to fit model field lines traced from 5.9 R_J to the Io footprint in the ionosphere, although the model did not constrain the longitudinal position of the mapped Io footprint. The model name reflects the fact that Voyager magnetometer data, Io footprint

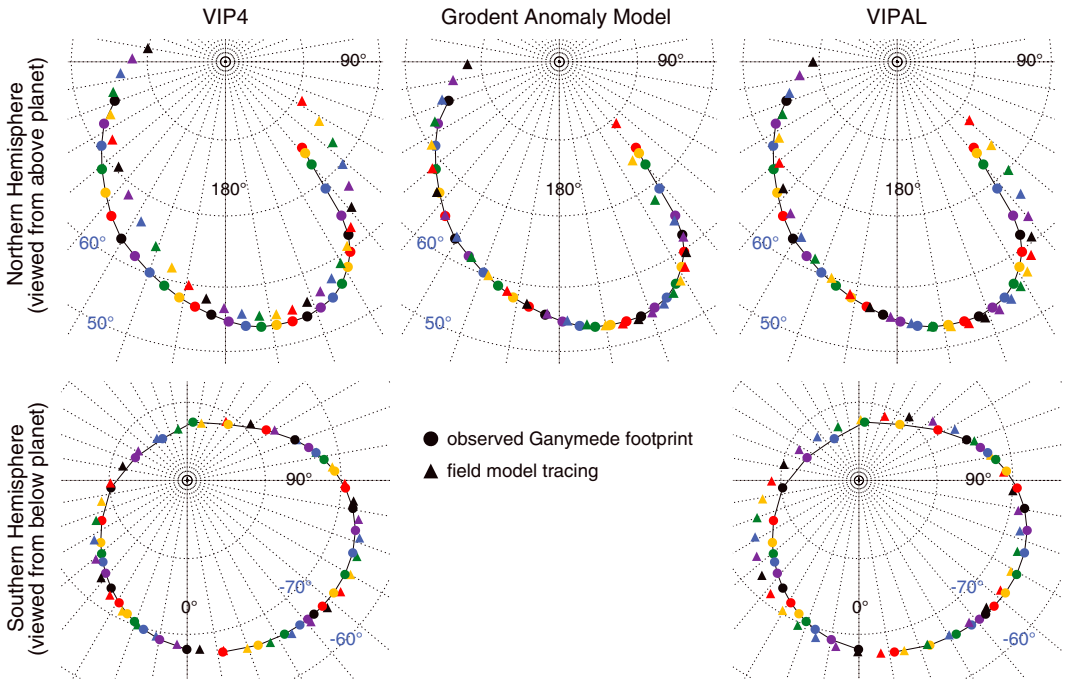

Figure 2. Ionospheric positions of the observed Ganymede footprint (circles) and the positions predicted by tracing model field lines from 15 R_J in the equator (triangles) using the VIP4, GAM, and VIPAL internal field models. Points are separated by 10° longitude at the equator. The repeating sequence of colors is used to guide the eye so that the observed footprint locations (circles) should be compared to the nearest model prediction point (triangles) of the same color. Modified from *Vogt and Kivelson* [2012].

observations, and Pioneer 11 magnetometer were used to calculate the fits for the internal field parameters (although Ulysses magnetometer data were also used). The VIP4 model generally matches the observed Io footprint location well, except in the northern hemisphere kink sector which gives the Io footprint its characteristic kidney bean shape.

The Grodent Anomaly Model [*Grodent et al*., 2008b], which we refer to as GAM, was designed as a proof of principle to show that the agreement between the model and footprint observations, particularly in the kink sector, could be improved by inclusion of a magnetic anomaly. Therefore, the model is applicable only to the northern hemisphere. *Grodent et al*. [2008b] presented two possible solutions for the location and orientation of the magnetic anomaly, which is represented by an additional dipole located close to the surface. In *Vogt et al*.'s [2011] model and in this study, we use the solution that located the additional dipole poleward of the Io footpath.

Most recently, *Hess et al*. [2011] published a model called VIPAL. The name reflects the fact that VIPAL is an update on VIP4 that models the magnetic Anomaly and places Longitudinal constraints on the mapping of the Io footprint. This model is applicable to both northern and southern hemispheres. The surface magnetic field strength predicted by VIPAL is in better agreement with values inferred from radio emissions than the surface field strength predicted by GAM.

The choice of an internal field model is important to our mapping because it affects the flux equivalence calculation in two ways. The first is that the internal field model is used to determine the 15 R_J reference contour, which should be located near the observed Ganymede footprint. Figure 2 compares the locations of the observed Ganymede footprint to that predicted by tracing field lines from the VIP4, GAM, and VIPAL models, in both the northern and southern hemispheres. Figure 2 shows that VIPAL matches the Ganymede footprint in the northern hemisphere better than both VIP4 and GAM. In the northern hemisphere, the GAM and VIPAL models match the observed footprints better than VIP4, particularly in the kink sector near 140° longitude and at longitudes ~190–220°. The mean spherical distance between the observed Ganymede footprint and the points predicted from tracing the model field lines to the northern hemisphere is 5.04° for

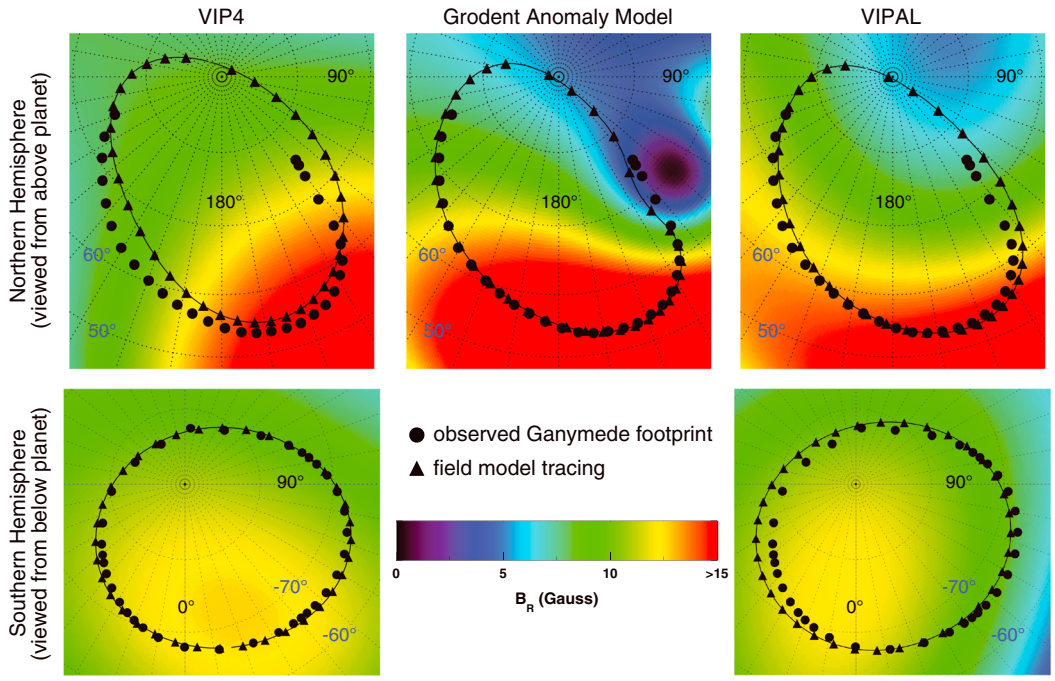

Figure 3. Strength of $B_{R,\mathrm{ion}}$, the radial magnetic field component in the ionosphere, from three different internal field models: VIP4, GAM, and VIPAL. The locations of the observed Ganymede footprint (circles) and the footprints of model field lines traced from 15 R_J in the equator (triangles) are shown in black.

VIP4, 3.52° for GAM, and 3.31° for VIPAL. The points traced from both GAM and VIPAL match the observed footprint locations in latitude, or distance normal to the Ganymede footpath, better than the points traced from VIP4. The GAM local time, or longitudinal, error is ~0.7 h, about twice the error of VIPAL, although VIPAL does not match the latitude of the Ganymede footprint as well as GAM at longitudes of ~140–150° and ~210–270°. In the southern hemisphere, VIP4 matches the Ganymede footprint better than VIPAL, particularly the latitudinal position at longitudes ~200–340°. The mean spherical distance between the observed Ganymede footprint and the points predicted from tracing the model field lines to the southern hemisphere is 2.33° for VIP4 and 3.27° for VIPAL.

The second way in which the choice of internal field model affects the flux equivalence calculation is in the strength of $B_{R,\mathrm{ion}}$, which affects the flux through the ionosphere. Figure 3 shows the modeled $B_{R,\mathrm{ion}}$ at a surface of 0.95 R_J for VIP4, GAM, and VIPAL, with the Ganymede footprint and modeled locations superimposed for reference. Most notably, in the northern hemisphere, the GAM predicts a higher $B_{R,\mathrm{ion}}$ than the other two models do for much of the area inside of the Ganymede footprint, and VIPAL predicts a much lower $B_{R,\mathrm{ion}}$ than VIP4 at high latitudes. Each model predicts a similar average $B_{R,\mathrm{ion}}$ inside the Ganymede footprint in the northern hemisphere—10.9 Gauss for VIP4, 11.1 Gauss for GAM, 10.3 Gauss for VIPAL—although the value of $B_{R,\mathrm{ion}}$ at a specific point can vary by more than a factor of 2 among the three models. The maximum $B_{R,\mathrm{ion}}$ values are 15.5 Gauss for VIP4, 18.8 Gauss for GAM, and 15.7 Gauss for VIPAL. All three models include similar amounts of flux inside (poleward of) the Ganymede footprint: ~1430 GWb for VIP4, ~1450 GWb for GAM, and ~1420 GWb for VIPAL in the northern hemisphere and ~1430 GWb for both VIP4 and VIPAL in the southern hemisphere ($1\,\mathrm{G} = 10^{-4}\,\mathrm{T}$, $1\,\mathrm{Wb} = \mathrm{T\,m^2}$).

Each internal field model has its relative strengths and weaknesses that will affect the flux equivalence calculation and resulting ionospheric mapping. Specifically, differences in the location of the initial 15 R_J contour and the modeled $B_{R,\mathrm{ion}}$ strength will shift the location and shape of the mapped ionospheric contours and the open/closed field line boundary. Our goal is to quantify how these shifts affect the magnetospheric mapping of specific points in the ionosphere and vice versa. Because all three models include a similar amount of flux inside the Ganymede footprint, we do not expect the choice of field model to significantly affect the predicted amount of open flux within the polar cap.

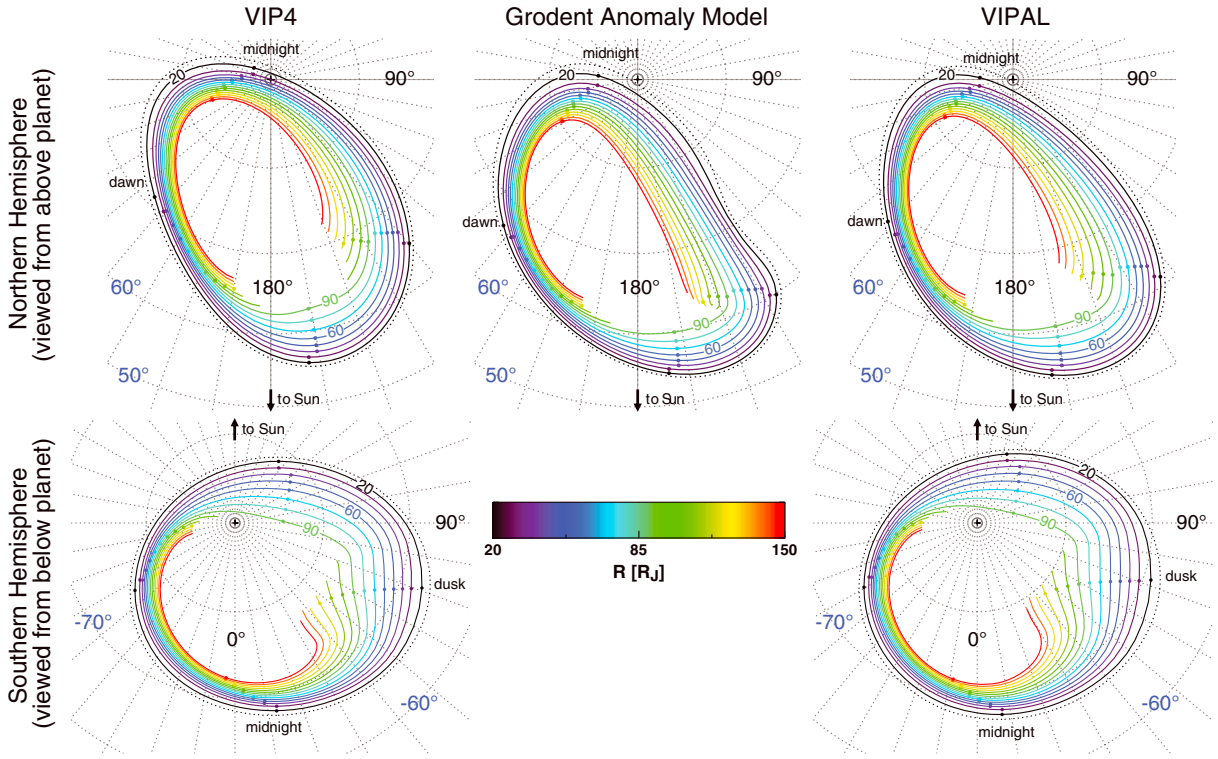

Figure 4. Ionospheric mapping contours for VIP4, GAM, and VIPAL, assuming subsolar longitude 180°, following the format of Figure 1 (bottom). The colors indicate the equatorial distances to which the contours map, every 10 R_J from 20 (black) to 150 (red) R_J. In the northern hemisphere, local noon is to the bottom of the page, with dawn and dusk to the left and right, respectively. The southern hemisphere (bottom) is drawn as seen by an observer looking up at the planet, with dawn and dusk to the left and right, respectively, as for the northern hemisphere, although local noon is to the top of the page.

4. Mapping Results: Comparison of the Three Different Field Models

4.1. Overview

We have performed the flux equivalence calculation described in section 2 in both the northern and southern hemispheres using the VIP4, GAM, and VIPAL internal field models. An error made in *Vogt et al.*'s [2011] southern hemisphere mapping has been corrected [*Vogt et al.*, 2011; corrected online 29 Dec. 2014]. Figure 4 shows an example of the resulting ionospheric contours, assuming a subsolar longitude of 180°, in 10 R_J increments from 20 to 150 R_J. The white region inside the colored ionospheric contours maps to distances beyond the dayside magnetopause or beyond 150 R_J on the nightside, and we identify this region as the polar cap. An overlay of the contours is shown in Figure 5. Tables 1 and 2 list several properties of the three models and the resulting ionospheric mappings for the northern and southern hemispheres, respectively.

Overall, the ionospheric contours calculated using the three different internal field models have similar morphology. Each case clearly features the dawn-dusk asymmetry in the contour spacing that arises because of the local time dependence of $B_{N,eq}$ and skews the polar cap location toward dawn local time. In the southern hemisphere, this leads to some sharp kinks, for example, in the 150 R_J contour (red) near dusk. The flux equivalence calculation predicts a similar polar cap size, equivalent to a symmetric circle around the pole with a ~9–11° latitudinal width, although the location of the polar cap differs for the various internal field models, as does the location of specific ionospheric contours. All models predict similar amounts of open flux in the polar cap, ~520–570 GWb.

The most striking differences between the mapping contours obtained using the VIP4 and GAM models, overlaid in the top left of Figure 5, result principally from large differences in the location of the 15 R_J contour. The initial 15 R_J contour, which is fixed in SIII longitude, differs by as much as ~7.6° (spherical distance) in the northern hemisphere for these two models, with an average difference of 3.6°. This initial difference shifts all of the subsequent ionospheric contours by several degrees. At this subsolar longitude,

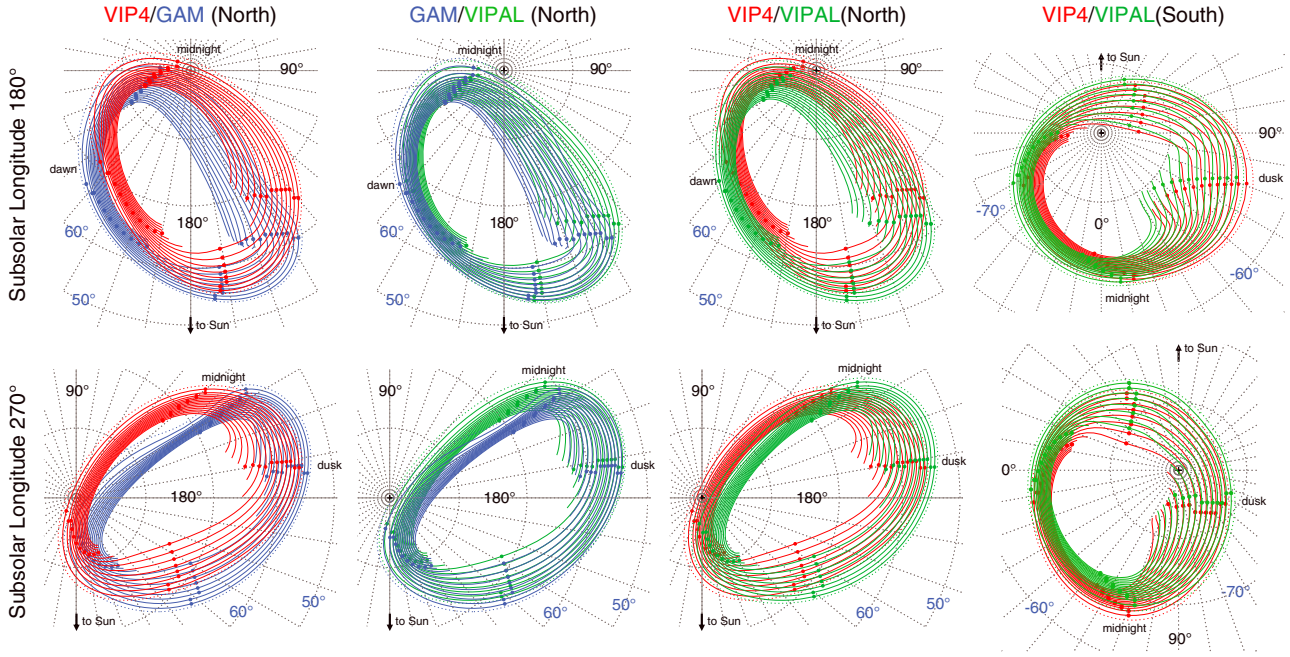

Figure 5. Overlay of the mapping contours calculated using the VIP4 (red), GAM (blue), and VIPAL (green) internal field models for subsolar longitude (top) 180° and (bottom) 270°, following the format of Figure 4.

the initial shift particularly affects the ionospheric mapping of points near dawn and dusk in the equator. For example, consider the contours between 200 and 220° longitude in the northern hemisphere. These ionospheric positions map to closed field lines at radial distances of 20–150 R_J and local times between ~04:00 and 08:00 LT with VIP4, but with GAM, nearly all of the points would map to radial distances beyond 150 R_J and would therefore be considered to be on open field lines.

By comparison, the GAM and VIPAL mappings agree relatively well, largely because of the similarity in the ionospheric traces of the 15 R_J contour. The initial 15 R_J contours from the two models differ on average by a spherical distance of just 1.4°, compared to 3.6° for VIP4/GAM or 2.7° for VIP4/VIPAL in the northern hemisphere. Considering all subsolar longitudes and radial distances 20–150 R_J, the mean spherical distance between two ionospheric points with the same equatorial mapping is 3.8° for VIP4/GAM, 1.5° for GAM/VIPAL, 2.8° for VIP4/VIPAL in the northern hemisphere, and 1.8° for VIP4/VIPAL in the southern hemisphere.

The few degree difference in the ionospheric contours for each of the three models typically corresponds to a difference of ~30 R_J and less than 1 h of local time in the mapped magnetospheric location of the same ionospheric point. For example, consider the points along the 30 R_J ionospheric contour as calculated using VIPAL in the northern hemisphere with subsolar longitude 180°. These points map from inside 15 R_J to ~90 R_J using VIP4 and from inside 15 R_J to ~85 R_J with GAM, as shown in Figure 6. Similarly, the points along the 30 R_J ionospheric contour with VIPAL in the southern hemisphere at subsolar longitude 180°

Table 1. Comparison of Various Properties of the Internal Field Models and Resulting Ionospheric Mappings in the Northern Hemisphere

Model	VIP4	GAM	VIPAL
Reference	*Connerney et al.* [1998]	*Grodent et al.* [2008b]	*Hess et al.* [2011]
Mean spherical distance between the observed Ganymede footprint and position predicted by tracing model field lines	5.04°	3.52°	3.31°
Flux inside (poleward of) the Ganymede footprint (GWb)	~1430	~1450	~1420
Area inside the Ganymede footprint	0.256 R_J^2	0.257 R_J^2	0.270 R_J^2
Typical radial field strength inside the Ganymede footprint (Gauss)	10.9	11.1	10.3
Typical field magnitude inside the Ganymede footprint (Gauss)	11.3	12.3	10.9
Polar cap open flux (GWb)	~540	~570	~520
Polar cap size equivalent (assuming a circle around the pole)	~10.3°	~10.0°	~10.3°

Table 2. Comparison of Various Properties of the Internal Field Models and Resulting Ionospheric Mappings in the Southern Hemisphere

Model	VIP4	VIPAL
Mean spherical distance between the observed Ganymede footprint and position predicted by tracing model field lines	2.33°	3.27°
Flux inside the Ganymede footprint (GWb)	~1430	~1430
Area inside the Ganymede footprint	0.242 R_J^2	0.254 R_J^2
Typical radial field strength inside the Ganymede footprint (Gauss)	11.5	11.0
Typical field magnitude inside the Ganymede footprint (Gauss)	11.7	11.3
Polar cap open flux (GWb)	~540	~540
Polar cap size equivalent (assuming a circle around the pole)	~9.7°	~9.7°

would map from inside 15 R_J to ~55 R_J with VIP4. Considering all ionospheric contours mapping from 20 to 150 R_J and all subsolar longitudes, the mean magnetospheric difference between points with the same ionospheric mapping is 38 R_J and 1.1 h of local time for VIP4/GAM, 19 R_J and 0.6 h of local time for GAM/VIPAL, 35 R_J and 0.8 h of local time VIP4/VIPAL in the north, and 25 R_J and 0.6 h of local time for VIP4/VIPAL in the south.

Thus far in our discussion, we have compared mapping contours with subsolar longitude 180°. Northern hemisphere auroral observations from HST are generally restricted to central meridian longitudes of ~110–260° because of Jupiter's ~10° dipole tilt. Therefore, 180° is an appropriate representative subsolar

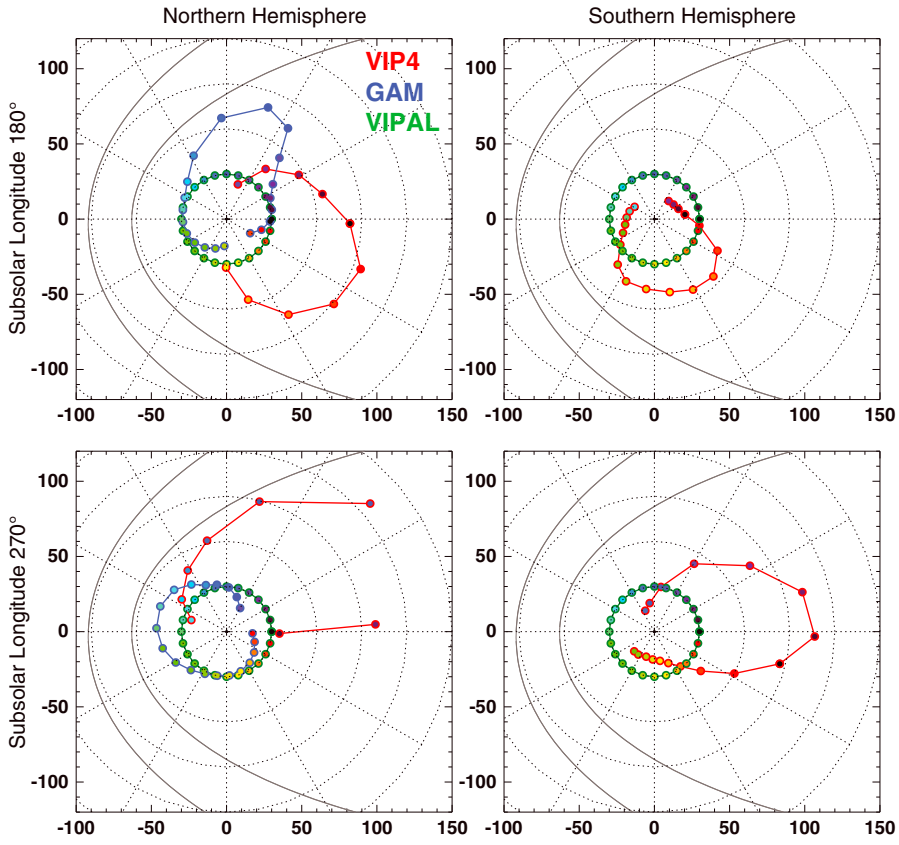

Figure 6. Equatorial magnetospheric mapping of the ionospheric locations in the (left) northern and (right) southern hemisphere that map to 30 R_J with VIPAL, shown here for subsolar longitudes (top) 180° and (bottom) 270°. The VIP4 mapping is shown in red, GAM in blue, and VIPAL in green. Individual points should be compared to those with the same interior color. Gaps in the VIP4 and GAM contours indicate where the mapped position is inside a radial distance of 15 R_J or beyond 150 R_J. The black lines show the compressed and expanded magnetopause locations of *Joy et al.* [2002]. The Sun is to the left.

longitude on which to focus our discussion. In Figure 5, however, we also present overlays of the ionospheric mapping contours for subsolar longitude 270° to illustrate that the most prominent differences among the various internal field model mappings are fixed in longitude and are not local time effects. For example, for both subsolar longitude 180° (Figure 5, top) and subsolar longitude 270°, the differences between the VIP4 and GAM mapping contours are most pronounced at longitudes ~140–160° and ~190–220° in the northern hemisphere, which is roughly where the modeled VIP4 15 R_J contour and the observed Ganymede footprint show the largest disagreement. These longitude ranges map roughly to dusk and dawn, respectively, at subsolar longitude 180° but to near midnight and noon at subsolar longitude 270°. Similarly, the differences between the mappings obtained with VIP4 and VIPAL in the south differ in the dawn-dusk direction at subsolar longitude 180° and in the noon-midnight direction at subsolar longitude 270°. In Figure 6 we plot the equatorial mapping for subsolar longitudes 180° and 270°, and show that the disagreement among the models is predominantly in the dawn-dusk direction for subsolar longitude 180° and in the noon-midnight direction for subsolar longitude 270°, for both the northern and southern hemispheres. This shows that the differences in mapping results obtained from the three models is primarily due to differences in how each model maps the Ganymede footprint.

Our results underscore the importance of using an accurate Jovian internal field model in *Vogt et al.*'s [2011] flux equivalence calculation. We have shown that the choice of field model typically affects the mapping results by a few degrees in the ionosphere or tens of Jovian radii and 1 h of local time in the magnetosphere. These shifts represent an uncertainty, or possible error, in the flux equivalence mapping results. However, it is important to note that these errors are strongly affected by inaccuracies in the Jovian internal field model and are not specific to the flux equivalence mapping approach. Our model is most accurate when mapping to or from ionospheric positions where the internal field models provide a good match to the observed Ganymede footprint: for the north, longitudes ~170–180° for VIP4, ~155–175° with GAM, and ~145–180° with VIPAL; and for the south, longitudes ~0–40°, ~70–100°, and ~320–360° with VIP4 and ~0–10°, ~40°, and ~340–360° with VIPAL. In these regions, the difference between the observed and modeled Ganymede footprints is typically less than 2° in spherical distance, and the expected error in the flux equivalence mapping is minimal.

4.2. Mapping Auroral Features

We turn now to a discussion of how the choice of internal field model affects the mapping of specific auroral features or regions. It is important to understand differences among the contours obtained with different field models that may influence our interpretation of the underlying magnetospheric processes, for example, differences in the mapped local time sector or radial position with respect to the magnetopause or a statistical X line. Similarly, when results from all three internal field models roughly agree, we can have greater confidence in the mapping accuracy of that specific point or feature.

Jupiter's main auroral emission is associated with a corotation enforcement current system that arises to accelerate outward moving logenic plasma back up to corotation in the middle magnetosphere [*Cowley and Bunce*, 2001; *Hill*, 2001]. Multiple theoretical studies have calculated the magnetospheric location of the expected field-aligned currents and their ionospheric mapping, based on assumptions about the magnetic field, plasma azimuthal velocity, radial mass transport rate, ionospheric conductivity, and other properties [e.g., *Cowley and Bunce*, 2001, 2003a, 2003b; *Hill*, 1979, 2001; *Nichols*, 2011; *Ray et al*., 2010]. However, only a few observational or theoretical studies [e.g., *Radioti et al*., 2008a; *Ray et al*., 2014] have considered how the observed local time variations in the plasma velocity and magnetic field structure will affect the ionospheric position of the main emission and its mapped radial distance in the magnetosphere. Therefore, one interesting application of the flux equivalence mapping is to identify the magnetospheric mapping of the main emission and particularly its dependence on local time.

Vogt et al. [2011] found that the flux equivalence calculation using the GAM internal field model mapped the main emission to larger distances (~50–60 R_J) postnoon than near dawn (~15–30 R_J). This local time trend appears to be common to the flux mapping with all three internal field models. Figure 7 shows the equatorial mapping of *Nichols et al.*'s [2009] main emission reference contour for VIP4 (red), GAM (blue), and VIPAL (green), assuming subsolar longitude 180°. This reference contour is based on the average location of the main emission in nearly 1000 HST images, all with subsolar longitudes between 140 and 220°, from 2007. Its coordinates are shown by the red line in Figure 7 (left) and are listed in Table 1 of *Nichols et al.* [2009]. Each point on the reference main emission maps to a specific point in the equatorial magnetosphere, but it should

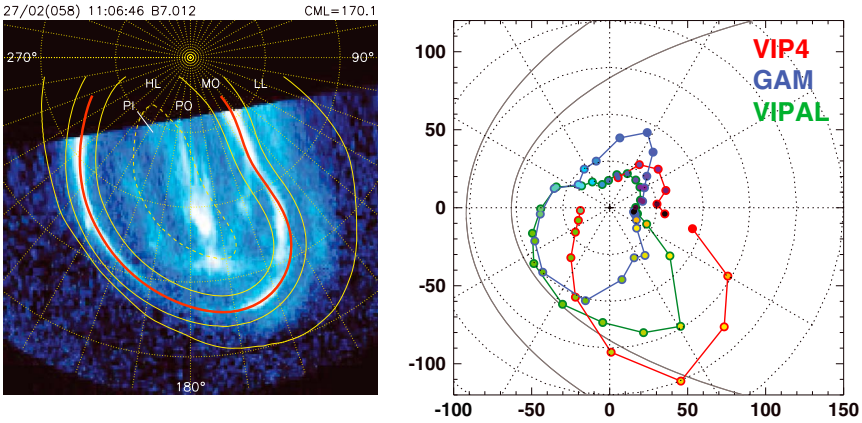

Figure 7. (left) An HST image of Jupiter's northern aurora, shown here in a polar projection. The red line is a reference main emission based on the average location in nearly 1000 HST images taken in 2007. Modified from *Nichols et al.* [2009, Figure 1]. (right) Mapped equatorial positions of *Nichols et al.*'s [2009] reference main emission contour for VIP4 (red), GAM (blue), and VIPAL (green), assuming subsolar longitude 180°. The small circles are drawn for each coordinate listed in Table 1 of *Nichols et al.* [2009], and the fill color varies from black to red for comparison among the three models. The black lines show the compressed and expanded magnetopause locations of *Joy et al.* [2002]. The Sun is to the left.

be noted that the main emission has a latitudinal width of ~1–3° [*Grodent et al.*, 2003a] so that the main emission maps to an extended range of radial distances. For all three internal field models, the reference main emission contour maps to larger radial distances near dusk than near dawn. At local times between noon and dusk, the mapping from all three models places the reference main emission contour maps near the *Joy et al.*'s [2002] compressed magnetopause. However, it is unlikely that the duskside main emission maps to the open/closed field line boundary. It is likely that the mapping overestimates the radial distance because the reference main emission contour is averaged from images when the magnetosphere was both expanded and compressed. The exceptionally large distances predicted with VIPAL and VIP4 (as far as ~90 and 120 R_J, respectively) in the postdusk sector are certainly overestimates resulting from the poor agreement between the VIP4 and VIPAL modeled 15 R_J contour and the observed Ganymede footprint in the ionospheric kink region, which maps roughly to dusk/postdusk at this subsolar longitude. The GAM and VIPAL flux calculations map the reference main emission to an average radial distance of ~35–40 R_J, consistent with expectations based on theoretical modeling. The average distance is slightly larger for VIP4, ~50 R_J, but still roughly consistent with expectations. Based on the calculated peak of field-aligned currents modeled under various conditions, the main emission is generally expected to map to the middle magnetosphere, with estimates ranging from ~30 R_J [*Hill*, 2001] to ~30–50 R_J [*Cowley and Bunce*, 2001] and to ~40–60 R_J [*Nichols*, 2011]. The fact that all three models map the main emission to larger distances near dusk than near dawn suggests that the corotation enforcement current peaks farther out in that local time sector and is an interesting observation for future study.

Another application of *Vogt et al.*'s [2011] mapping with the GAM flux equivalence calculation was to map the location of the three polar auroral regions, described above in section 2 [*Vogt et al.*, 2011]. The shapes and locations of the dark, swirl, and active regions were shown to vary with time and subsolar longitude. The active region was found to map to open field lines near and beyond the dayside magnetopause and the swirl region mapped to open field lines beyond 150 R_J on the night side, for two HST images taken at subsolar longitudes 160° and 220°. However, the dark region's mapping differed for different HST images: at subsolar longitude 156°, it mapped to predawn open and closed field lines, while at subsolar longitude 270°, it mapped to predawn open field lines.

The GAM contours are shown in Figure 8 (blue contours), which also shows the mapping obtained using the flux equivalence calculation with VIP4 (red contours) and VIPAL (green contours). All models map the swirl region (identified by the red dashed line) to nightside open field lines at both subsolar longitudes, supporting the interpretation of the swirl region as Jupiter's polar cap. However, the models do not fully agree for the active or dark regions at the two subsolar longitudes. For subsolar longitude 156°, all models map the active region (identified by the green dashed line) to open field lines beyond the dayside magnetopause, but for subsolar longitude 220°, VIP4 maps most of the active region to closed field lines near noon. Additionally, the

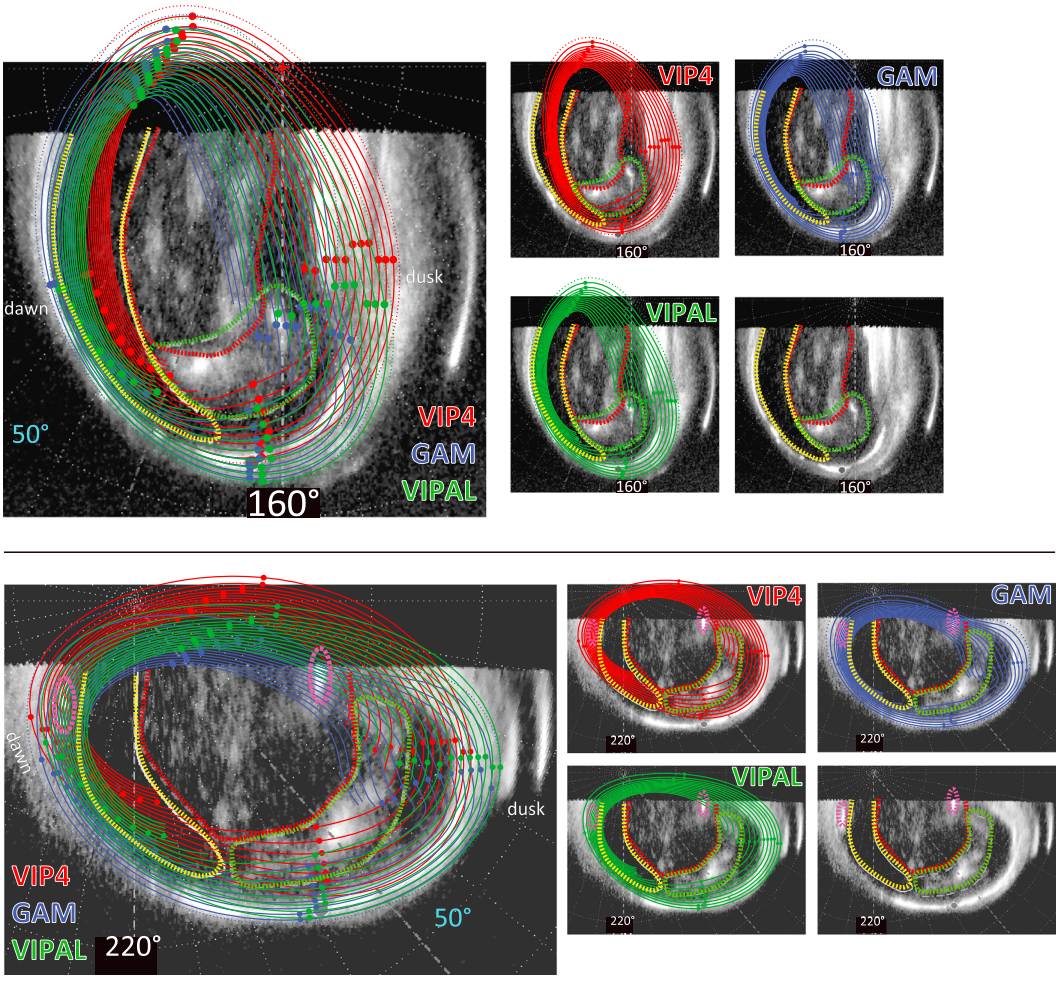

Figure 8. Comparison of HST auroral observations and mapping results from VIP4 (red), GAM (blue), and VIPAL (green), shown here in a polar view for central meridian longitude (CML) (top) 160° and (bottom) 202°. The Sun's direction is toward the bottom of the page. The polar dark, active, and swirl regions are highlighted by the yellow, green, and red dashed contours, respectively. In the image taken at CML 202° (bottom), two polar spots, one dawn spot and one nightside spot, are highlighted by the pink dashed lines. Following *Vogt et al.* [2011, Figures 14 and 15].

dark region mapping varies significantly among the models, being almost entirely on closed predawn field lines with VIP4 and on both open and closed field lines for VIPAL, for both subsolar longitudes 156° and 220°. Because VIP4 does not match the Ganymede footprint well at longitudes ~190°–220°, the mapping using VIP4 for the dark region at subsolar longitude 156° and for the active region at subsolar longitude 220° is probably less accurate than the mapping of those regions with GAM or VIPAL, which place the dark region on both open and closed field lines.

Finally, we examine the mapping of polar dawn spots, thought to be associated with inward moving flow from tail reconnection [*Radioti et al.*, 2010]. This is based in part on their emitted power, recurrence time, and location just poleward of the main emission and in the dawn local time sector. Most reconnection signatures reported in particle and magnetic field data have been observed in the predawn local time sector [*Kronberg et al.*, 2005; *Vogt et al.*, 2010], where theoretical studies suggest that both the solar wind-driven Dungey cycle and the rotationally driven Vasyliūnas cycle would be active [*Vasyliūnas*, 1983; *Cowley et al.*, 2003]. An example of a polar dawn spot from February 2007 is shown in Figure 9 (left). If the polar dawn spots are the signature of inward moving flow from reconnection, they should map to radial distances close to and inside of the statistical X lines defined by *Woch et al.* [2002] using particle bursts and by *Vogt et al.* [2010] using magnetic field data. These two statistical X lines are located near 90 R_J predawn and at larger radial distances at earlier local times, as shown in Figure 9 (right).

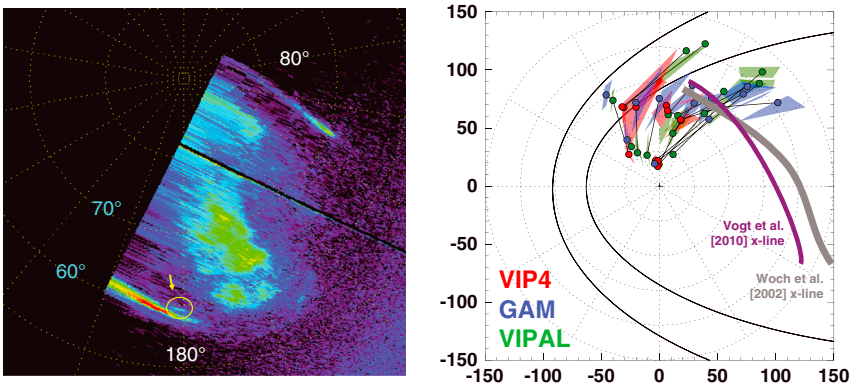

Figure 9. (left) Polar projection of a northern hemisphere auroral image from HST, with a polar dawn spot highlighted in yellow, just poleward of the main emission. This image was taken at CML 115.9° and subsolar longitude 126.4° so that the direction toward the Sun is to the lower right. (right) Equatorial mapping of 19 polar dawn spots determined with the flux equivalence calculation with VIP4 (red), GAM (blue), and VIPAL (green). Mappings are not shown if the spot mapped to inside 15 R_J, beyond 150 R_J, or outside the magnetopause. The shaded regions indicate the 3 pixel uncertainty in the spot's ionospheric location. The solid black lines connect the positions mapped with the various field models for the same spot. *Vogt et al.*'s [2010] and *Woch et al.*'s [2002] statistical X lines are drawn in purple and gray, respectively. The black lines show the compressed and expanded magnetopause locations of *Joy et al.* [2002]. The Sun is to the left.

Using the flux equivalence calculation with the three internal field models, we mapped 19 polar dawn spots observed in 2007 from the northern ionosphere to the magnetosphere. The polar dawn spots are observed to last as long as tens of hours [*Radioti et al.*, 2008b] and can therefore be observed in consecutive HST images. In this work we use the spot position identified from one image so that no spot is counted twice. The spots' ionospheric positions, subsolar longitudes, and mapped locations with each model are provided as online supporting information. The spots are located at longitudes 173°–243°, including 8 spots at longitudes 190°–220° where the VIP4 model does not match the observed Ganymede footprint well, and we therefore expect that the most reliable mapping will come from GAM and VIPAL. The mapped magnetospheric positions from VIP4 (red), GAM (blue), and VIPAL (green) are plotted in Figure 9 (right). The shaded colored regions indicate the 3 pixel uncertainty in identifying the spot location on the original HST image. In some cases, a 3 pixel uncertainty was located beyond the planet's limb and therefore could not be defined. Figure 9 (right) does not show spots mapped to inside 15 R_J (8 spots with VIP4 and 1 spot with VIPAL) or spots mapped to outside the magnetopause or beyond 150 R_J (7 spots with GAM and 2 spots with VIPAL). The spot shown in Figure 9 (left) maps to ~70 R_J and ~05:40 LT with VIP4 and to beyond the dayside magnetopause with GAM and VIPAL.

For all three field models, the mapping of most spots is generally consistent with their association with inward moving flow from tail reconnection. All models map most spots to distances inside of the statistical X lines (19 of 19 with VIP4, 9 of 19 with GAM, and 12 of 19 with VIPAL, including spots mapped to inside 15 R_J). All models place the spots at local times ~03:00 to 08:00, whereas the occurrence frequency of observed reconnection events peaks earlier, at ~02:00 to 04:00 [*Vogt et al.*, 2010]. That the polar dawn spots do not map to earlier local times is possibly due to auroral viewing geometries that make it difficult to analyze much of the nightside aurora because it is located near or beyond the limb (e.g., Figure 8) and the fact that our study has neglected nightside auroral spots, which have also been observed and associated with premidnight reconnection signatures [e.g., *Grodent et al.*, 2004; *Radioti et al.*, 2011]. It should be noted that the statistical X line is an average of nearly 250 observed reconnection events and that reconnection events where B_θ is positive, suggesting planetward flow, have been observed at distances from 33 to 145 R_J, with a median distance of ~62 R_J [*Vogt et al.*, 2010]. The spots' mapped locations with GAM and VIPAL are therefore broadly consistent with the observed reconnection events. The mapping with VIP4 is the least consistent with the observations because it places most spots inside 30 R_J and at local times later than ~04:50.

For the spots that map outside the magnetopause, there are two likely explanations. The first is that the spots are the result of tail reconnection but there is an error in the mapping, possibly due to the fact that the flux equivalence calculation is generic and has not accounted for temporal variability in the solar wind or

current sheet parameters. The second possibility is that these polar dawn spots are the signature of a process other than tail reconnection, such as small-scale turbulent interactions with the solar wind that arise due to the Kelvin-Helmholtz Instability [e.g., *Delamere and Bagenal*, 2010].

5. Summary and Conclusions

The flux equivalence calculation of *Vogt et al*. [2011] provides a way to relate polar auroral features to their source regions in Jupiter's middle and outer magnetosphere. It is based on the requirement that the flux threading a region in the magnetosphere must equal the flux through the region in the ionosphere to which it maps. The calculation begins by tracing model field lines from 15 R_J in the magnetosphere to the ionosphere, where models can be tested against Ganymede's auroral footprint. It then calculates the flux through the magnetosphere, using a fit to magnetic field data that accounts for variation in radial distance and local time, and matches this to the radial flux through the ionosphere. While this flux equivalence method is more reliable than tracing field lines from a global field model, it still requires an internal field model to identify the 15 R_J ionospheric reference contour and to estimate the radial field through the ionosphere at latitudes higher than that of the Ganymede footprint. There are three widely used models of Jupiter's internal field—VIP4, the Grodent Anomaly Model or GAM, and VIPAL—and the purpose of this study was to quantify how the choice of internal field model affects the mapping results of the flux equivalence calculation. We have not considered how the mapping may change in response to temporal variations in the mass loading rate from Io or changing solar wind conditions, although these would be interesting topics for future study.

We have shown that the choice of internal field model can lead to significant shifts in the flux equivalence mapping of identical points, and we have quantified these differences. For mapping from the magnetosphere to the ionosphere, the mapped ionospheric position of two identical magnetospheric positions differs by an average of ~2–3° in spherical distance, but the difference can be as large as ~8°. The mapped magnetospheric location of two identical points in the ionosphere typically differs by ~30 R_J and less than 1 h in local time, but the difference can be more than 100 R_J and nearly 6 h in local time. The differences introduced by the use of different internal field models result in part from the accuracy with which the models represent the 15 R_J contour traced by the ionospheric footprint of Ganymede, since the three models predict similar average values of $B_{R,\mathrm{ion}}$ in our area of interest. While the value of $B_{R,\mathrm{ion}}$ at a specific point can vary by more than a factor of 2 among the three models, all three models include similar amounts of flux inside the Ganymede footprint and therefore also similar amounts of open flux in the polar cap. The initial 15 R_J contours for each model differ from each other by a typical spherical distance of ~1–3°, with larger differences in the northern auroral kink sector, which is not well reproduced by VIP4 or VIPAL, and at longitudes from ~190 to 220° in the northern hemisphere or ~200–340° in the southern hemisphere. The differences among the various internal field model mappings are therefore fixed in longitude and are not local time effects.

We then considered whether the flux equivalence mapping of specific auroral features differed significantly with each of the three models, which could alter the interpretation of the underlying physical processes. The flux equivalence mapping with all three models indicates that *Nichols et al*.'s [2009] reference main auroral emission maps to increasingly large distances with increasing local time from dawn to dusk and predicts average radial distances that are consistent with expectations based on theoretical modeling. Additionally, we compared the mappings of the three polar auroral regions from two sample HST images and found that the flux equivalence calculation with all three field models maps the swirl region to nightside magnetic field lines beyond 150 R_J. The GAM and VIPAL mappings of the dark and active regions show general agreement, placing the active region on open field lines just beyond the dayside magnetopause and the dark region mostly on open field lines. Finally, we examined the mappings of 19 polar dawn spots and found that their mapped locations using all three field models are generally consistent with their association with inward moving flow from tail reconnection.

Our findings highlight the importance of using the most accurate internal field model available for mapping between Jupiter's ionosphere and the magnetosphere with *Vogt et al*.'s [2011] flux equivalence approach. The mapping uncertainties we have described here are strongly affected by inaccuracies in the internal field models and are not specific to the flux equivalence calculation. In general, field lines traced using VIPAL provide the best match to the observed Ganymede footprint in the northern hemisphere, although

VIPAL does not match the latitude of the Ganymede footprint as well as GAM at longitudes of ~140–150° and ~210–270°. VIP4 matches the observed Ganymede footprint better than VIPAL in the southern hemisphere. However, all models have a mean error between the observed and modeled Ganymede footprint location equivalent to at least 2° in spherical distance.

We look to the Juno mission, scheduled to arrive at Jupiter in 2016, whose observations should lead to the development of a more accurate Jovian internal field model. Until then, the uncertainties described in our study should be accounted for in the continued analysis of HST images of Jupiter's aurora and the planning of observations during the Juno mission.

Acknowledgments

This study was motivated in part by constructive criticism given by Fran Bagenal and Peter Delamere and several spirited discussions with them regarding the mapping model published in *Vogt et al.* [2011]. We gratefully acknowledge Paul Withers for carefully reading the manuscript and providing helpful comments. Mapping results can be obtained via a webform at http://www.igpp.ucla.edu/people/mvogt/mapping/ or with IDL code that can be obtained by contacting M.F.V. We gratefully acknowledge Benjamin Palmaerts for testing this IDL code, which was used extensively in the analysis for this study. M.F.V. and E.J.B. were supported by the UK Science and Technology Facilities Council Consolidated grant ST/K001000/1. This work was completed while R.J.W. served at the National Science Foundation as Program Director for Magnetospheric Physics as part of the Individual Research and Development program.

Larry Kepko thanks the reviewers for their assistance in evaluating this paper.

References

Bagenal, F., et al. (2014), Magnetospheric science objectives of the Juno mission, *Space Sci. Rev.*, doi:10.1007/s11214-014-0036-8.

Bonfond, B. (2013), When moons create aurora: The satellite footprints on giant planets, in *Auroral Phenomenology and Magnetospheric Processes: Earth and Other Planets*, *Geophys. Monogr. Ser.*, vol. 197, edited by A. Keiling et al., pp. 133–140, AGU, Washington, D. C., doi:10.1029/2011GM001169.

Bonfond, B., D. Grodent, J.-C. Gérard, T. Stallard, J. T. Clarke, M. Yoneda, A. Radioti, and J. Gustin (2012), Auroral evidence of Io's control over the magnetosphere of Jupiter, *Geophys. Res. Lett.*, *39*, L01105, doi:10.1029/2011GL050253.

Broadfoot, A. L., et al. (1979), Extreme ultraviolet observations from Voyager 1 encounter with Jupiter, *Science*, *204*, 979–982.

Bunce, E. J., S. W. H. Cowley, and T. K. Yeoman (2004), Jovian cusp processes: Implications for the polar aurora, *J. Geophys. Res.*, *109*, A09S13, doi:10.1029/2003JA010280.

Clarke, J. T., et al. (2002), Ultraviolet emissions from the magnetic footprints of Io, Ganymede, and Europa on Jupiter, *Nature*, *415*, 997–1000.

Connerney, J., M. Acuña, and N. Ness (1981), Modeling the Jovian current sheet and inner magnetosphere, *J. Geophys. Res.*, *86*(A10), 8370–8384, doi:10.1029/JA086iA10p08370.

Connerney, J. E. P., R. Baron, T. Satoh, and T. Owen (1993), Images of excited H_3^+ at the foot of the Io flux tube in Jupiter's atmosphere, *Science*, *262*, 1035–1038.

Connerney, J. E. P., M. H. Acuña, N. F. Ness, and T. Satoh (1998), New models of Jupiter's magnetic field constrained by the Io flux tube footprint, *J. Geophys. Res.*, *103*, 11,929–11,939, doi:10.1029/97JA03726.

Cowley, S. W. H., and E. J. Bunce (2001), Origin of the main auroral oval in Jupiter's coupled magnetosphere-ionosphere system, *Planet. Space Sci.*, *49*, 1067–1088.

Cowley, S. W. H., and E. J. Bunce (2003a), Modulation of Jovian middle magnetosphere currents and auroral precipitation by solar wind-induced compressions and expansions of the magnetosphere: Initial response and steady state, *Planet. Space Sci.*, *51*, 31–56.

Cowley, S. W. H., and E. J. Bunce (2003b), Modulation of Jupiter's main auroral oval emissions by solar wind-induced expansions and compressions of the magnetosphere, *Planet. Space Sci.*, *51*, 57–79.

Cowley, S. W. H., E. J. Bunce, T. S. Stallard, and S. Miller (2003), Jupiter's polar ionospheric flows: Theoretical interpretation, *Geophys. Res. Lett.*, *30*(5), 1220, doi:10.1029/2002GL016030.

Delamere, P. A., and F. Bagenal (2010), Solar wind interaction with Jupiter's magnetosphere, *J. Geophys. Res.*, *115*, A10201, doi:10.1029/2010JA015347.

Gérard, J.-C., D. Grodent, A. Radioti, B. Bonfond, and J. T. Clarke (2013), Hubble observations of Jupiter's north-south conjugate ultraviolet aurora, *Icarus*, *226*, 1559–1567.

Grodent, D. (2014), A brief review of ultraviolet auroral emissions on giant planets, *Space Sci. Rev.*, doi:10.1007/s11214-014-0052-8.

Grodent, D., J. T. Clarke, J. Kim, J. H. Waite, and S. W. H. Cowley (2003a), Jupiter's main auroral oval observed with HST-STIS, *J. Geophys. Res.*, *108*(A11), 1389, doi:10.1029/2003JA009921.

Grodent, D., J. T. Clarke, J. H. Waite Jr., S. W. H. Cowley, J.-C. Gérard, and J. Kim (2003b), Jupiter's polar auroral emissions, *J. Geophys. Res.*, *108*(A10), 1366, doi:10.1029/2003JA010017.

Grodent, D., J.-C. Gérard, J. T. Clarke, G. R. Gladstone, and J. H. Waite (2004), A possible auroral signature of a magnetotail reconnection process on Jupiter, *J. Geophys. Res.*, *109*, A05201, doi:10.1029/2003JA010341.

Grodent, D., J.-C. Gérard, A. Radioti, B. Bonfond, and A. Saglam (2008a), Jupiter's changing auroral location, *J. Geophys. Res.*, *113*, A01206, doi:10.1029/2007JA012601.

Grodent, D., B. Bonfond, J.-C. Gérard, A. Radioti, J. Gustin, J. T. Clarke, J. Nichols, and J. E. P. Connerney (2008b), Auroral evidence of a localized magnetic anomaly in Jupiter's northern hemisphere, *J. Geophys. Res.*, *113*, A09201, doi:10.1029/2008JA013185.

Hanlon, P. G., M. K. Dougherty, N. Krupp, K. C. Hansen, F. J. Crary, D. T. Young, and G. Tóth (2004), Dual spacecraft observations of a compression event within the Jovian magnetosphere: Signatures of externally triggered supercorotation?, *J. Geophys. Res.*, *109*, A09S09, doi:10.1029/2003JA010116.

Hess, S. L. G., B. Bonfond, P. Zarka, and D. Grodent (2011), Model of the Jovian magnetic field topology constrained by the Io auroral emissions, *J. Geophys. Res.*, *116*, A05217, doi:10.1029/2010JA016262.

Hill, T. W. (1979), Inertial limit on corotation, *J. Geophys. Res.*, *84*(A11), 6554–6558, doi:10.1029/JA084iA11p06554.

Hill, T. W. (2001), The Jovian auroral oval, *J. Geophys. Res.*, *106*, 8101–8107, doi:10.1029/2000JA000302.

Joy, S. P., M. G. Kivelson, R. J. Walker, K. K. Khurana, C. T. Russell, and T. Ogino (2002), Probabilistic models of the Jovian magnetopause and bow shock locations, *J. Geophys. Res.*, *107*(A10), 1309, doi:10.1029/2001JA009146.

Khurana, K. K. (2001), Influence of solar wind of Jupiter's magnetosphere deduced from currents in the equatorial plane, *J. Geophys. Res.*, *106*, 25,999–26,016, doi:10.1029/2000JA000352.

Kivelson, M. G., and K. K. Khurana (2002), Properties of the magnetic field in the Jovian magnetotail, *J. Geophys. Res.*, *107*(A8), 1196, doi:10.1029/2001JA000249.

Kronberg, E. A., J. Woch, N. Krupp, A. Lagg, K. K. Khurana, and K.-H. Glassmeier (2005), Mass release at Jupiter: Substorm-like processes in the Jovian magnetotail, *J. Geophys. Res.*, *110*, A03211, doi:10.1029/2004JA010777.

Nichols, J. D. (2011), Magnetosphere-ionosphere coupling in Jupiter's middle magnetosphere: Computations including a self-consistent current sheet magnetic field model, *J. Geophys. Res.*, *116*, A10232, doi:10.1029/2011JA016922.

Nichols, J. D., J. T. Clarke, J. C. Gérard, D. Grodent, and K. C. Hansen (2009), Variation of different components of Jupiter's auroral emission, *J. Geophys. Res.*, *114*, A06210, doi:10.1029/2009JA014051.

Pallier, L., and R. Prangé (2001), More about the structure of the high-latitude Jovian aurorae, *Planet. Space Sci.*, *49*, 1159–1173.
Radioti, A., J.-C. Gérard, D. Grodent, B. Bonfond, N. Krupp, and J. Woch (2008a), Discontinuity in Jupiter's main auroral oval, *J. Geophys. Res.*, *113*, A01215, doi:10.1029/2007JA012610.
Radioti, A., D. Grodent, J.-C. Gérard, B. Bonfond, and J. T. Clarke (2008b), Auroral polar dawn spots: Signatures of internally driven reconnection processes at Jupiter's magnetotail, *Geophys. Res. Lett.*, *35*, L03104, doi:10.1029/2007GL032460.
Radioti, A., D. Grodent, J.-C. Gérard, and B. Bonfond (2010), Auroral signatures of flow bursts released during magnetotail reconnection at Jupiter, *J. Geophys. Res.*, *115*, A07214, doi:10.1029/2009JA014844.
Radioti, A., D. Grodent, J.-C. Gérard, M. F. Vogt, M. Lystrup, and B. Bonfond (2011), Nightside reconnection at Jupiter: Auroral and magnetic field observations from July 26, 1998, *J. Geophys. Res.*, *116*, A03221, doi:10.1029/2010JA016200.
Ray, L. C., R. E. Ergun, P. A. Delamere, and F. Bagenal (2010), Magnetosphere-ionosphere coupling at Jupiter: Effect of field-aligned potentials on angular momentum transport, *J. Geophys. Res.*, *115*, A09211, doi:10.1029/2010JA015423.
Ray, L. C., N. A. Achilleos, M. F. Vogt, and J. N. Yates (2014), Local time variations in Jupiter's magnetosphere-ionosphere coupling system, *J. Geophys. Res. Space Physics*, *119*, 4740–4751, doi:10.1002/2014JA019941.
Russell, C. T., Z. J. Yu, K. K. Khurana, and M. G. Kivelson (2001), Magnetic field changes in the inner magnetosphere of Jupiter, *Adv. Space Res.*, *28*(6), 897–902.
Stallard, T. S., S. Miller, S. W. H. Cowley, and E. J. Bunce (2003), Jupiter's polar ionospheric flows: Measured intensity and velocity variations poleward of the main auroral oval, *Geophys. Res. Lett.*, *30*(5), 1221, doi:10.1029/2002GL016031.
Tao, C., R. Kataoka, H. Fukunishi, Y. Takahashi, and T. Yokoyama (2005), Magnetic field variations in the Jovian magnetotail induced by solar wind dynamic pressure enhancements, *J. Geophys. Res.*, *110*, A11208, doi:10.1029/2004JA010959.
Vasyliūnas, V. M. (1983), Plasma distribution and flow, in *Physics of the Jovian Magnetosphere*, edited by A. J. Dessler, p. 395, Cambridge Univ. Press, New York.
Vogt, M. F., and M. G. Kivelson (2012), Relating Jupiter's auroral features to magnetospheric sources, in *Auroral Phenomenology and Magnetospheric Processes: Earth and Other Planets*, edited by A. Keiling et al., AGU, Washington, D. C., doi:10.1029/2011GM001181.
Vogt, M. F., M. G. Kivelson, K. K. Khurana, S. P. Joy, and R. J. Walker (2010), Reconnection and flows in the Jovian magnetotail as inferred from magnetometer observations, *J. Geophys. Res.*, *115*, A06219, doi:10.1029/2009JA015098.
Vogt, M. F., M. G. Kivelson, K. K. Khurana, R. J. Walker, B. Bonfond, D. Grodent, and A. Radioti (2011), Improved mapping of Jupiter's auroral features to magnetospheric sources, *J. Geophys. Res.*, *116*, A03220, doi:10.1029/2010JA016148.
Waite, J. H., Jr., et al. (2001), An auroral flare at Jupiter, *Nature*, *410*, 787–789.
Woch, J., N. Krupp, and A. Lagg (2002), Particle bursts in the Jovian magnetosphere: Evidence for a near-Jupiter neutral line, *Geophys. Res. Lett.*, *29*(7), 1138, doi:10.1029/2001GL014080.